Supplementary Materials: Baddeleyite as a widespread and sensitive indicator of bombardment in planetary crusts

White, L. F., Darling, J.R., Moser, D., Cayron, C., Barker. I., Dunlop, J., & Tait, K. T.

Additional Sample Details

In total five polished thin sections and one grain mount were examined during this study. All samples were polished using a 50nm alumina agent with a Buehler Vibromat II vibratory polisher. The range of unshocked baddeleyite structures were defined using four grains within a single thin section of the Anna's Rust Sill (02-154; E 37 31 12, S 26 50 42), two mm-scale grains from the Phalaborwa carbonatite complex (Heaman 2009), South Africa, and three grains from a single thin section (MDS002) of the Matachewan dyke swarm, Ontario, Canada. Single polished thin sections of three shocked mafic samples of the Matachewan diabese dyke swarm, sampled in increasing proximity to the remnant Sudbury impact melt sheet, provided the contextualized shocked samples incorporated into this study. UTM grid references for these samples are provided in Supplementary Table 1.

Sample	Locality	Shock State	UTM (Zone 17)
JD12SUD14	Matachewan	Shocked	0460596, 5163552
JD12SUD06	Matachewan	Shocked	0458468, 519129
JD12SUD03	Matachewan	Shocked	0464642, 5164223
MDS002	Matachewan	Unshocked	0448954, 534877
U-Pb Standard Mount	Phalaborwa	Unshocked	See notes*
02-154	Anna's Rust Sill	Unshocked	See notes*

Supplementary Table 1: *Overview of sample localities.*

A first-order insight into the shock state of these samples can be gathered in the field, where cross-cutting relationships, pseudotachylyte veins and shattercones can place constraints on the P-T histories experienced by the samples. Within the most proximal samples (JD12SUD14 & JD12SUD15), shattercones within the mafic dyke provide an empirical > 2 GPa pressure estimate (Osinski & Ferrière 2016). The apex of the observed cone appears to point towards the local interface with the melt sheet (S/SE). Although reported up to ~10km north of the melt sheet (Deutsch et al. 1995; Grieve & Therriault, 2000), convincing shattercones were not observed in association with the other sample localities. Pseudotachylyte bands and veins were commonly observed, varying in thickness from ~3 cm to < 50 m. Finer veins contain predominately local clasts, subsampling the immediately surrounding target rocks, while coarser bands appear to transport entrained clasts further. Pseudotachylyte thickness also appears to control roundness of clasts, with thinner veins preserving sharp inclusions and thicker bands producing more rounded clasts. Along the dyke - granite contact, localized frictional movement has generated a small pseudotachylyte vein of sheared and mobilized mafic clasts within a felsic belt. Such relationships provide additional insight into the brittle response of the crust during impact events, and further constrain shock pressures to > 6 GPa (Kenkmann et al. 2000).

Supplementary Figure 1: *Field photographs depicting a shattercone within the Matachewan dyke (sample JD12SUD14;* ***A****) and the pseudotachylytic contact between the dyke and host felsic material (****B****). Both features are diagnostic of shock deformation of the target rocks associated with an impact event.*

Optical microscopy (conducted using a petrological microscope at the University of Portsmouth) reveals further details on the genesis and deformation of the collected samples. The Matachewan dyke swarm is predominately doleritic in composition (plagioclase laths (< 1.5 cm), augite, ± baddeleyite), though has been variably overprinted by greenschist facies metamorphism (chlorite, epidote, actinolite). Feldspar appears crystalline (highlighting an absence of high pressure diaplectic maskelynite), though is cloudy in PPL. Planar feature are absent even within the most impact proximal plagioclase, while extinction appears slightly strained in all samples. Augite crystals appear highly cracked and fractured, and contain < 20 um thick planar features shown to crosscut twin lamellae at approximately ~100°. Such structures have been observed in other shocked pyroxene grains (Short 1970), but formative P-T conditions are poorly constrained. Other phases, such as chlorite, show no obvious signs of shock deformation, instead crystallizing during post-impact metamorphism.

Supplementary Figure 2: *Optical image of sample JD12SUD14 taken under crossed polarized light (XPL). Augite (orange / blue birefringence) displays numerous crack and fracture patterns, in addition to largely planar features cross cutting the grain. Feldspar diffracts, though appears cloudy.*

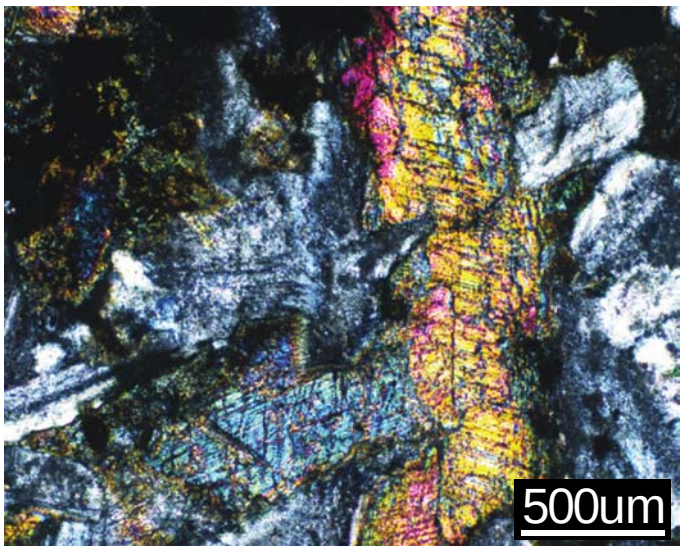

Additional scanning electron microscopy (SEM) methods

Target baddeleyite grains were located and imaged using a combination of automated backscatter electron (BSE) and energy-dispersive X-ray spectroscopy (EDS) techniques using the Oxford Instruments INCA and Aztec 'Feature' modules and Oxford X-Max 80 detectors installed on electron microscopes at the University of Portsmouth, UK and the Zircon and Accessory Phase Laboratory (ZAPlab) at the University of Western Ontario, Canada. Grains were imaged using BSE and secondary electron (SE) techniques, and micro- to nano-scale structural analysis was conducted by electron backscatter diffraction (EBSD), using Oxford Instruments Nordlys EBSD detectors mounted on either a Hitachi SU6600 field emission gun SEM (FEG-SEM; ZAPLab) or Zeiss EVO MA10 LaB_6-SEM (Portsmouth). Generated baddeleyite diffraction patterns were matched to inorganic crystal structure database (ICSD) card 15,983 using crystal lattice parameters of $\alpha = 5.21$, $\beta = 5.26$, $\gamma = 5.37$, and $\alpha° = 90°$, $\beta° = 80.5°$, $\gamma° = 90°$ (Smith & Newkirk 1965). Wild spike reduction was completed on all EBSD datasets, although no other form of raw data correction was conducted. Full instrument details can be found in Supplementary Table 2.

Instrumentation		
Host Institute	Western University	Portsmouth University
SEM Model	Hitachi SU6600 FEG-SEM (Schottky electron source)	Zeiss EVO MA10 (LaB_6 electron source)
EBSD System	Oxford Instruments Nordlys EBSD detector	Oxford Instrument Nordlys-Nano EBSD detector
EBSD Software	HKL Channel 5	Oxford Instruments AZTEC
SEM settings		
Carbon coat (<5nm)	Yes	No
Acc. Voltage (kV)	20	20
Working distance (mm)	19	14 to 20
Probe current (nA)	8	1
EBSD data collection and processing		
EBSP collection time per frame (ms)	80	< 120
Background (frames)	64	64
EBSP noise reduction (frames)	7	5
EBSP noise reduction (binning)	4x4	2x2
EBSP noise reduction (gain)	High	High
Hough resolution	60	70
Band detection min/max	4 to 7	10 to 12
Step size (nm)	50 to 150	100 to 200
Noise reduction	wildspike only	wildspike only

Supplementary Table 2: *Overview of electron backscatter diffraction (EBSD) instrument and analytical conditions.*

Waste heat calculations to constrain shock temperatures

Near-instantaneous shock loading and release of a crystal lattice inherently generates waste heat within the material (i.e. Sharp & De Carli, 2006). An estimate of this waste heat can be generated by calculating the energy imparted on the lattice by the shock loading event via modelling of a range (0 – 5 km/s, increments of 0.01km/s) of particle velocities (U_p) for a material of known density. Mineral physics properties for baddeleyite were extracted from various sources (Supplementary Table 2), and an estimate for shock induced waste heat generated using the calculations of Sharp & DeCarli, 2006; Appendix A.

Sample Density (Mg/m^3)	Co (km/sec)	± ΔCo (km/sec)	S	± ΔS	lower Up (km/sec)	upper Up (km/sec)	Phase
5.814	5.17	0.08	1.02	0.05	0.41	2.17	Low-P
	4.42	0.07	1.35	0.03	2.17	2.99	High-P

Supplementary Table 2: *Equation of state parameters for baddeleyite from Mashimo et al., 1984 and Ahrens & Johnson, 1995. The transition from low-pressure phase data to high-pressure phase data occurs at ~2.28 km/s U_p; the point at which the two calculated Hugoniot curves smoothly intercept (i.e. Sharp & De Carli, 2006).*

Any shock-induced temperature increase for baddeleyite grains of the Matachewan dyke swarm must acknowledge the increased starting temperature of the dyke swarm at the time of impact. It is estimated that the North Range of Sudbury was approximately ~6 km deep at the time of impact (Pye et al., 1984; Spray et al., 2004); assuming a geothermal gradient of 25ºC / km (Martin, 1986), the rocks would have sat at approximately ~150ºC. Finally, the Grüneisen parameter (γ) must be factored in; a function of thermal expansion, bulk modulus and specific volume. For most rocks and minerals < 100 GPa, γ values are typically between 0.5 and ~2 (Sharp & De Carli, 2006). Here we model post-shock temperatures for shock loaded baddeleyite across two γ values (1 and 2) to produce an upper and lower estimate of waste-heat generation. However, this effect only accounts for a minimal variability in post shock temperature (~55ºC at 100 GPa).

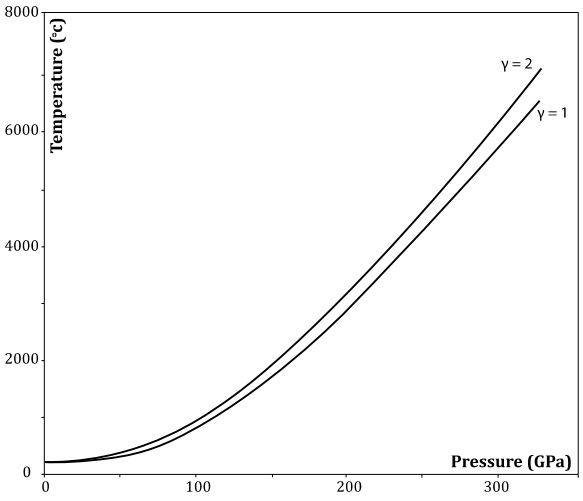

Supplementary Figure 3: *Waste heat curves for shock loaded baddeleyite (ZrO_2). Taking shock loading-related waste heat generation in isolation reveals pressures in excess of ~130 GPa must be achieved in order to generate the high-temperature tetragonal-ZrO_2 phase, while ~175 GPa would induce sufficient temperatures (~2500ºC) to form the cubic-ZrO_2 polymorph (Hannink et al., 2000).*

Additional EBSD insights into reversion twinning & phase heritage

In total, nine unshocked baddeleyite grains from three mafic localities were mapped using EBSD during this study. Grains in all samples yield crystallographically similar simple and polysynthetic twin relationships characterized by an ~18º rotation about the {001} plane (Supplementary Figure 4). These twins are lost in highly shocked baddeleyite grains which develop up to 15 unique twin relationships. Of these, only two twin relationships yield an 18º rotation in {001} space identical to unshocked igneous grains.

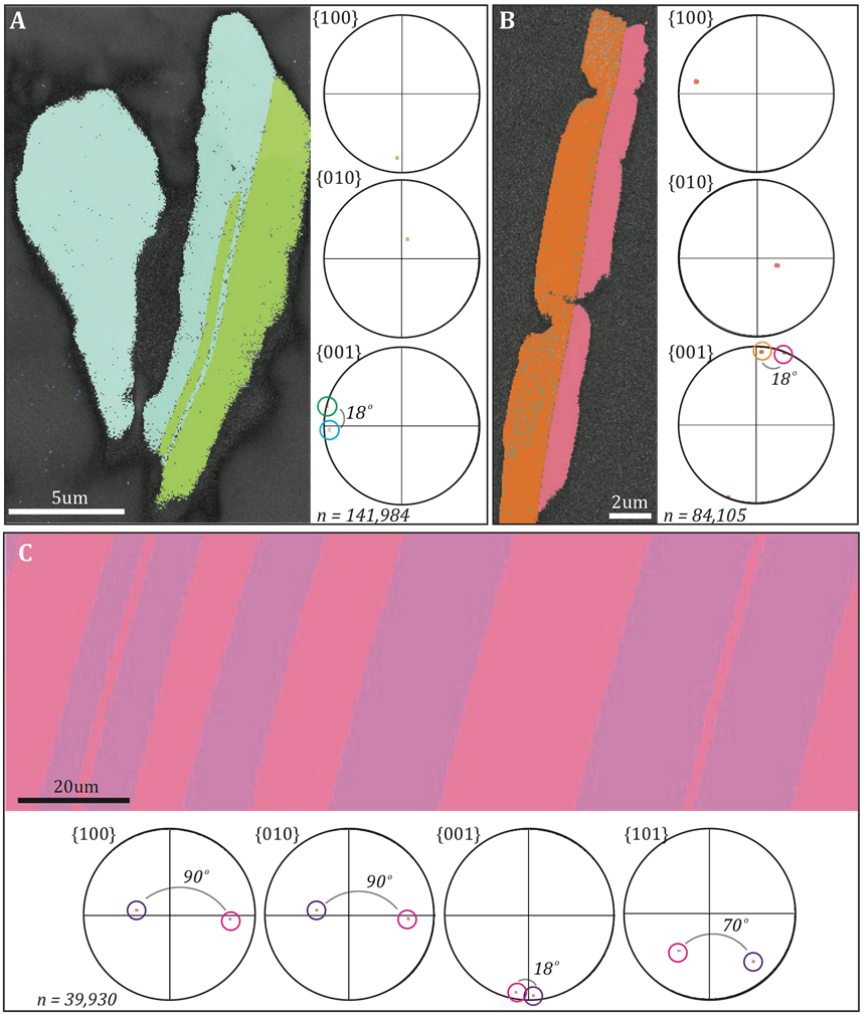

Supplementary Figure 4: *EBSD data (all euler map and pole figures) for unshocked baddeleyite grains sampled from the Anna's Rust Sill (**A**), unshocked Matachewan dyke swarm (**B**) and Phalaborwa carbonatite complex (**C**). Labelled semi-circles highlight angular misorientation between the crystallographic domains.*

Orthogonal relationships between the twin domains are clearly observed in {100}, {001}, {110} and {011} pole-to-plane space. This relationship is less pronounced in {010} space. This abundance and orientation of twin relationships can be used to infer the former presence and reversion of a ZrO_2 polymorph; either high temperature tetragonal or cubic structures, or high pressure orthorhombic structures. Given the structure of the orthorhombic crystal system (all angles = 90º; a ≠ b ≠c),

crystallographically constrained reversion of this phase to stable monoclinic grains would produce the observed subgrain relationships. However, reversion from the high temperature tetragonal phase would also account for the observed microstructure. Here, the presence of zircon microtwins in adjacent felsic material, and the estimated low waste heat temperatures generated in baddeleyite by the shock loading event, suggest the high pressure orthorhombic structure governs this reversion twinning. Later events would never induce the P-T conditions required to overprint this initial, impact-induced microstructure (Supplementary Table 3), preserving a robust record of shock metamorphism within the sample set.

Event	Pressure (GPa)	Temperature (°C)	Evidence
Impact Event	> 19	~200	Zircon microtwins, waste heat estimates (*this study*)
Melt-sheet annealing	0.6 - 0.8	< 950	Thermal modeling (*James et al., 1992*)
Greenschist-facies metamorphism	< 1	< 500	Constrained by mineralogical assemblage (*Spray et al., 2004*)

Supplementary Table 3: *Overview of peak P-T conditions experienced by impact-proximal sample JD12SUD14. Despite undergoing a range of geological events, only high shock pressures (constrained by the presence of zircon microtwins to > 19 GPa) can induce a phase transformation of the ZrO_2 lattice.*

Phase reconstruction using the ARPGE software package

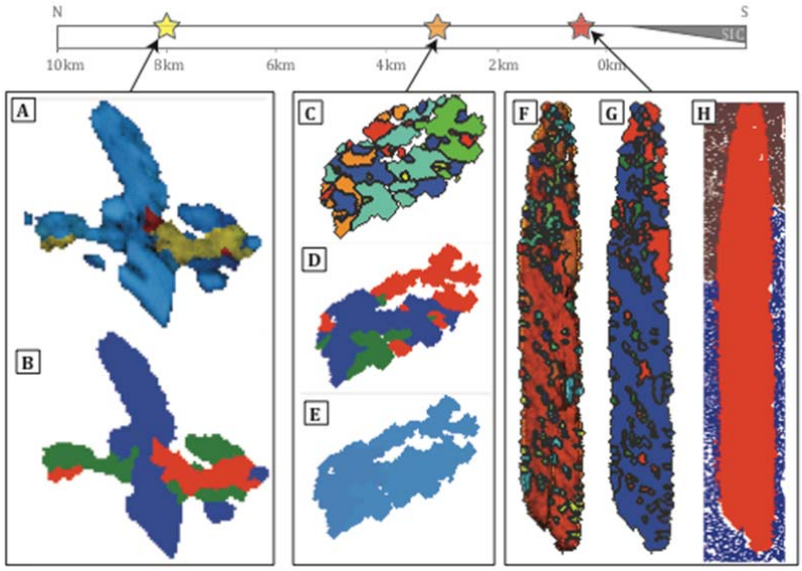

Supplementary Figure 5: *ARPGE phase reconstructions for key shocked grains. Monoclinic domains in JD12SUD06 (**A**) reconstruct into three unique tetragonal / orthorhombic packets (**B**), though one of these represents a preserved, igneous twinned baddeleyite grain, prohibiting reconstruction of the data to a higher symmetry parent. Monoclinic domains in JD12SUD03 (**C**) can be associated with three tetragonal / orthorhombic parent structures (**D**) and a single high symmetry precursor (**E**). The most highly shocked sample (JD12SUD14) is comprised of a multitude of unique monoclinic orientations (**F**) which can be associated with three tetragonal / orthorhombic parents (**G**) and a single high symmetry precursor (**H**).*

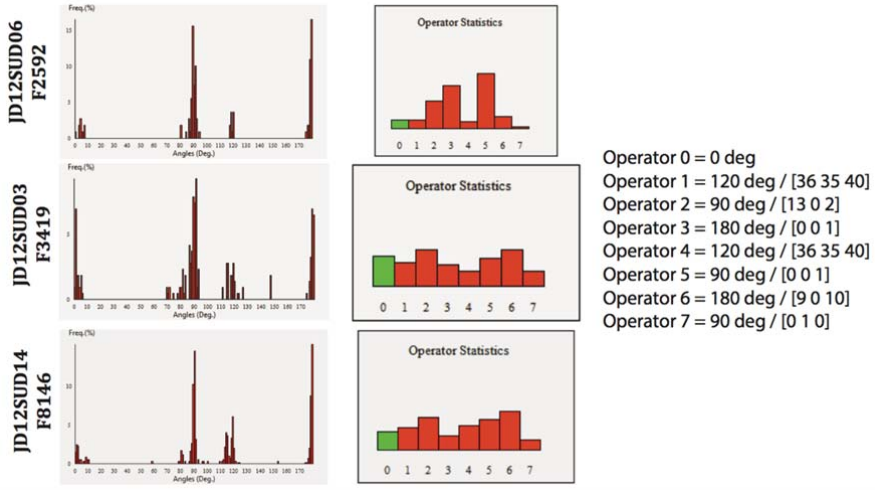

Supplementary Figure 6: *Operator statistics and misorientation histograms for EBSD datasets presented for shocked baddeleyite grains (Figure 2). The least shocked grain (JD12SUD06, F2592) displays minimal evidence of operators 4 and 7, yielding a peak at ~115° instead. Shocked grains display similar spreads of misorientation relationships, though peaks become more defined in the most highly shocked baddeleyite grains (sample JD12SUD14, F8146).*

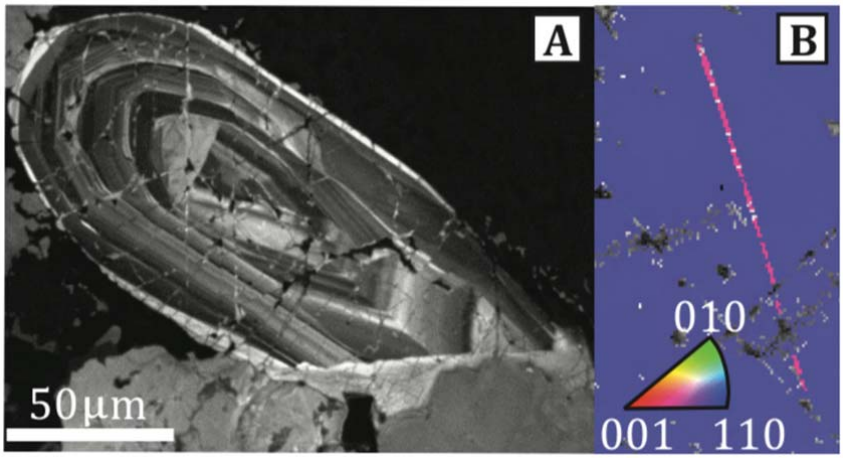

Supplementary Figure 7. *Cathodoluminescence image (A) and inverse pole figure (IPF) data (B) for impact-proximal (~0.55 km) zircon within zircon-bearing felsic intrusion sample JD12SUD15a (Matachewan dike swarm, Sudbury impact structure, Canada). Grain contains an abundance of diagnostic shock features, including pervasive planar deformation features and micro-twin lamella rotated 65°/<110>. Such features reveal the high shock pressure history of the North Range of Sudbury, placing empirical constraints (ca. 20 GPa; Timms et al., 2017) on microstructural features observed in adjacent baddeleyite.*

Additional References

Ahrens, T. J. & Johnson, M. L. 1995. Shock Wave Data for Minerals. *In: Mineral Physics and Crystallography: A handbook of physical constraints. (Ed: Ahrens, T.),* pp. 143 – 185. doi: 10.1029/RF002

Deutsch, A., Grieve, R. A. F., Avermann, M., Bischoff, L., Brockmeyer, P., Buhl, D., Lakomy, R., Müller-Mohr, V., Ostermann, M. and Stöffler, D. (1995) 'The Sudbury Structure (Ontario, Canada): a tectonically deformed multi-ring impact basin', *Geologische Rundschau*, 84(4), pp. 697–709.

Grieve, R. A. F., Therriault, A., 2000, Vredefort, Sudbury, Chicxulub: Three of a Kind?, *Annual Reviews of Earth and Planetary Science* **28**, 305 – 338.

Hannink, R.H.J., Kelly, P.M. & Muddle, B.C., 2000. Transformation Toughening in Zirconia-Containing Ceramics. *Journal of the American Ceramic Society*, 83(3), pp.461–487.

Kenkmann, T., Hornemann, U. and Stöffler, D. (2000) 'Experimental generation of shock-induced pseudotachylites along lithological interfaces', *Meteoritics & Planetary Science*, 35, pp. 1275–1290.

Martin, H. 1986. Effect of steeper Archean geothermal gradient on geochemistry of subduction-zone magmas. *Geology,* 14(9), pp. 753 – 756.

Mashimo, T., Nagayama, K. & Sawoka, A. 1983. Shock compression of zirconia ZrO_2 and zircon $ZrSiO_4$ in the pressure range up to 150 GPa. *Phys. Chem. Minerals* 9, pp. 237 – 247.

Osinski, G.R. & Ferrière, L., 2016. Shattercones : (Mis)understood? *Science Advances*, 2(8), pp.1–10.

Pye et al., in Giblin, P.E. and Naldrett, A.J. eds., 1984. *The geology and ore deposits of the Sudbury structure*. Ontario Ministry of Natural Resources.

Sharp, T. G. & de Carli, P. S. 2006. Shock Effects in Meteorites. *In: Meteorites and the Early Solar System II (Eds: Lauretta, D. S. & McSween, H. Y.),* University of Arizona Press, Tucson, pp. 653 – 677.

Short, N. M. (1970) 'Evidence and implications of shock metamoprhism in lunar samples', *Proceedings of the Apollo 11 Lunar Science Conference*, 1, pp. 865–871.

Spray, J. G., Butler, H. R. & Thompson, L. M. 2004. Tectonic influences on the morphology of the Sudbury impact structure: Implications for terrestrial cratering and modeling. *Meteoritics & Planetary Science,* 39(2), pp. 287 – 301.